Journal of Hazardous Materials, 30 (1992) 195–224
Elsevier Science Publishers B.V., Amsterdam

Numerical simulations of LNG vapor dispersion from a fenced storage area

S.T. Chan

University of California, Lawrence Livermore National Laboratory, P.O. Box 808, L-262 Livermore, CA 94551 USA

(Received December 15, 1990; accepted in revised form October 23, 1991)

Abstract

The FEM3A model, with minor modifications, has been applied to simulate the vapor dispersion of four large-scale LNG vapor barrier field experiments and a comparison was made with relevant field data. The model was able to reproduce the major results of the experiments within a factor of two under most circumstances. For Falcon-1, with additional heat flux over the source area to model the superheating effects, results consistent with field observations were obtained. In particular, a vapor cloud overfilling the fenced enclosure was reproduced, in contrast with a vapor cloud essentially contained within the fence at all times observed in a pre-spill wind tunnel simulation. The simple approach currently taken to model turbulence and heat transfer in the source area has performed reasonably well; however, more sophisticated modeling of the source may be necessary for more accurate predictions at all locations. Results from simulations of the Falcon-4 experiment indicate that an LNG vapor fence can significantly reduce the downwind distance and hazardous area of the flammable vapor clouds. However, a vapor fence could also prolong the cloud persistence time in the source area, thus increasing the potential for ignition and combustion within the vapor fence and the area nearby.

1. Introduction

In order to evaluate and eventually predict the possible mitigating effects of vapor fences on the dispersion of the vapor cloud resulting from an accidental liquefied natural gas (LNG) spill in storage areas, the U.S. Department of Transportation (DOT) and the Gas Research Institute (GRI) initiated a research program to evaluate methods for predicting LNG dispersion distances for realistic facility configurations. As part of the program, Lawrence Livermore National Laboratory (LLNL) conducted a series of large-scale field experiments called the "LNG Vapor Barrier Verification Field Trials" (also referred to as the "Falcon Series") at the U.S. Department of Energy's Liquefied

Correspondence to: Dr S.T. Chan, University of California, Lawrence Livermore National Laboratory, P.O. Box 808, L-262 Livermore, CA 94551 (USA).

Gaseous Fuels Spill Test Facility (LGFSTF), Nevada, in the summer of 1987. The objectives of the experiments were: (1) to provide a data base on LNG vapor dispersion from spills involving complex field obstacles to assist in validation of wind tunnel and mathematical models, and (2) to assess the effectiveness of vapor fences for mitigating LNG vapor dispersion hazards in the event of an accidental spill.

Five spill experiments were conducted, covering releases of LNG at rates of 9 to 30 m^3/min and spill volumes ranging from 21 to 66 m^3. The spills were conducted on water in order to generate vapor at rates equivalent to the liquid spill rates. To this end, a 40 m by 60 m recirculating pond was constructed (and filled with water to about 0.76 m in depth) at the end of the spill pipes from the LGFSTF. A 0.3-m diameter spill line was connected to a system of four 0.15-m diameter spill distribution lines (referred to as the spill "spider") to distribute rapidly spilling LNG across the pond surface. The pond was enclosed by a fiberglass vapor fence of 88 m long, 44 m wide, and 8.7 m high. In addition, a 17.1 m wide by 13.3 m high billboard-like barrier was erected upwind of the pond to generate turbulence due to obstructions such as a storage tank. A sketch of the vapor fence configuration is shown in Fig. 1 and a snapshot of the vapor cloud from the Falcon-4 test is shown in Fig. 2. Details of the experiments and field data can be found in the GRI Report No. 89/0138 [1].

Due to the complexity in the physics and geometry of the spill scenarios, wind tunnel modeling has generally been regarded as the best-suited, economical way for predicting the dispersion distances of hazardous concentrations of such LNG vapor clouds. However, under conditions of low wind speed, low

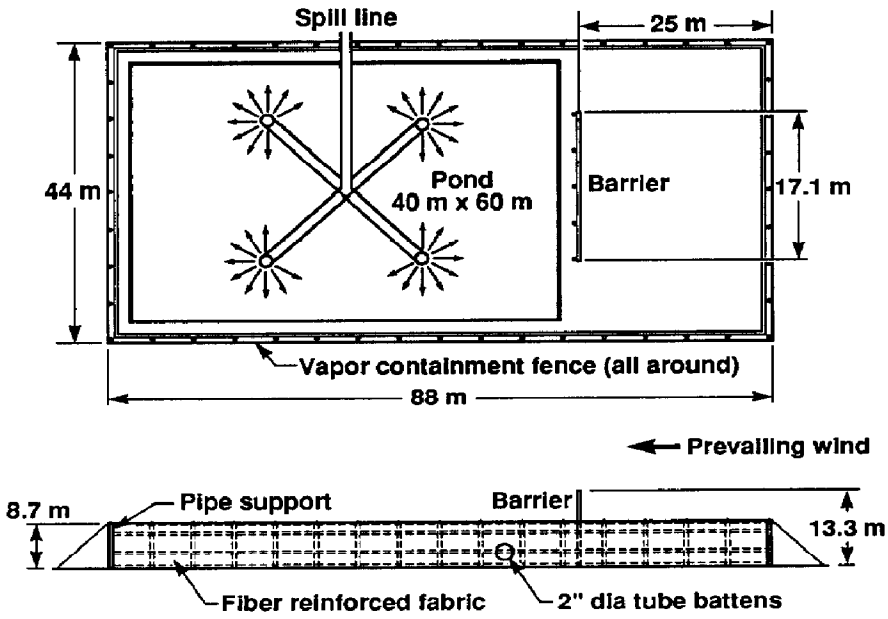

Fig. 1. Vapor fence configuration for the Falcon series spill experiments.

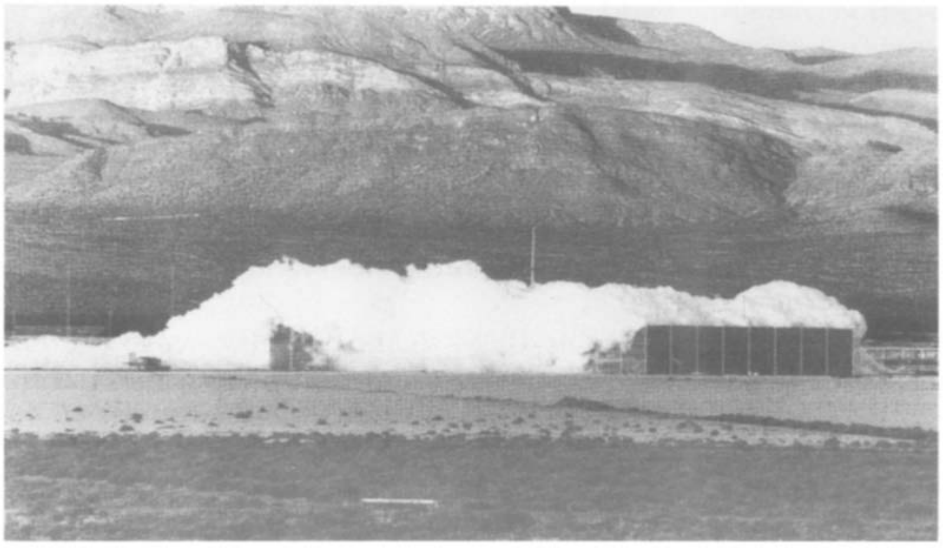

Fig. 2. LNG vapor cloud from the Falcon-4 experiment conducted at the U.S. Department of Energy's liquefied gaseous fuels spill test facility, Nevada, in the Summer of 1987.

level of turbulence, and significant heat transfer (which is usually true for LNG), wind tunnel modeling of such dense-gas plume has certain practical difficulties and is generally more contentious than a comparable positively buoyant release [2]. In fact, a pre-test wind tunnel simulation of the Falcon-1 test produced a vapor cloud which was essentially contained within the vapor fence for all times, which strongly contrasted with the Falcon-1 field release where the vapor cloud greatly overfilled the fenced enclosure.

In many cases, especially under the above circumstances, accurate three-dimensional (3-D) mathematical models can be an effective and complementary tool to wind tunnel modeling. With numerical models, the physical parameters can be controlled more easily and detailed temporal and spatial results can often provide insights into the physical processes involved in the cloud dispersion. Actually, the usefulness of currently available numerical models such as FEM3 for simulating a wide range of heavy-gas dispersion scenarios has already been demonstrated by Chan and Ermak [3] and Chan et al. [4]. Recently an improved version of FEM3, called FEM3A, was applied for the first time to evaluate the effectiveness of vapor fences for controlling LNG vapor dispersion [5].

In this paper, the major results and findings from a recent study using the FEM3A model to simulate the Falcon experiments [6] are reported. The objectives of the study were, through numerical modeling and a detailed model-data comparison: (1) to improve the understanding of LNG vapor dispersion involving barriers, (2) to assess FEM3A in modeling such complex vapor dispersion scenarios, and (3) to complement the results of field and wind tunnel

tests, such as providing plausible explanations for unexpected results and filling in data gaps due to instrument failure or limited array size. Toward these goals, relevant field measurements were analyzed and several series of 2-D and 3-D simulations were carried out. The 2-D simulations were performed mainly to improve our understanding of the physics involved in the spill scenarios and to aid the modeling of turbulence and heat transfer in the source area. The 3-D calculations were conducted to complement the field and wind tunnel experiments and to assess the performance of the numerical model for such vapor dispersion simulations.

In the following, several features of the FEM3A model relevant to the numerical simulations are described and a model-data comparison for the simulated tests in presented and discussed. Additionally, a brief assessment of the effectiveness of the vapor barrier is conducted for Falcon-4. Finally, some concluding remarks are presented in the last section.

2. The FEM3A model

In this section, certain salient features of the FEM3A model relevant to the present study are described. They include the governing equations, turbulence parameterization, source modeling and superheating effects. A more detailed description of the FEM3A model can be found in Chan [7].

2.1 Governing equations

The following three-dimensional, time-dependent conservation equations, written for the mean (time-averaged) quantities in a turbulent flow field, are being solved in FEM3A:

$$\frac{\partial(\rho \boldsymbol{u})}{\partial t}+\rho \boldsymbol{u}\cdot\nabla \mathbf{u}=-\nabla p+\nabla\cdot(\rho \mathbf{K}^{\mathrm{m}}\cdot\nabla \boldsymbol{u})+(\rho-\rho_{\mathrm{h}})\boldsymbol{g}\,, \tag{1}$$

$$\nabla\cdot(\rho \boldsymbol{u})=0\,, \tag{2}$$

$$\begin{aligned}\frac{\partial\theta}{\partial t}+\boldsymbol{u}\cdot\nabla\theta=&\frac{1}{\rho C_p}\nabla\cdot(\rho C_p\mathbf{K}^{\theta}\cdot\nabla\theta)\\&+\frac{C_{pv}-C_{pa}}{C_p}(\mathbf{K}^{\mathrm{c}}\cdot\nabla q_{\mathrm{v}})\cdot\nabla\theta\\&+\frac{C_{pl}-C_{pa}}{C_p}(\mathbf{K}^{\mathrm{c}}\cdot\nabla q_{\mathrm{l}})\cdot\nabla\theta-\frac{L}{C_p}\left(\frac{\partial q_{\mathrm{v}}}{\partial t}\right)_{\mathrm{pc}}\,,\end{aligned} \tag{3}$$

$$\frac{\partial q_{\mathrm{v}}}{\partial t}+\boldsymbol{u}\cdot\nabla q_{\mathrm{v}}=\frac{1}{\rho}\nabla\cdot(\rho\mathbf{K}^{\mathrm{c}}\cdot\nabla q_{\mathrm{v}})+\left(\frac{\partial q_{\mathrm{v}}}{\partial t}\right)_{\mathrm{pc}}\,, \tag{4}$$

$$\frac{\partial q_l}{\partial t} + \boldsymbol{u}\cdot\nabla q_l = \frac{1}{\rho}\nabla\cdot(\rho\mathbf{K}^c\cdot\nabla q_l) - \left(\frac{\partial q_v}{\partial t}\right)_{pc}, \tag{5}$$

and

$$\rho = \frac{PM}{RT} = \frac{PM_a}{RT\left[1+\left(\frac{M_a}{M_v}-1\right)q_v - q_l\right]}. \tag{6}$$

In the above equations, $\boldsymbol{u}$ denotes the velocity field $=(u,v,w)^T$; ρ the mixture density; p the pressure deviation from a hydrostatic pressure field (p_h) corresponding to a motionless state with constant lapse rate of temperature; ρ_h is the density field corresponding to the above motionless state; $\boldsymbol{g}$ the acceleration due to gravity $(g_x, g_y, g_z)^T$; θ the potential temperature deviation from an adiabatic atmosphere at θ_0 (the reference temperature); q_v, q_l are the mass fractions of material in vapor, and liquid phases; $\mathbf{K}^m$, $\mathbf{K}^\theta$, $\mathbf{K}^c$ are the eddy diffusion tenors for momentum, energy, and species, respectively; C_{pa}, C_{pv}, C_{pl} and C_p are the specific heats of the ambient atmosphere, the dispersed material in vapor phase, the liquid material, and the mixture, i.e. $C_{pv}q_v + C_{pl}q_l + (1-q_v-q_l)C_{pa}$, respectively; L is the latent heat of phase change for the dispersed material; ∇ is the gradient operator; t time; $(\partial q_v/\partial t)_{pc}$ is the time rate of change of material vapor due to phase change; M, M_a, M_v are the molecular weights of the mixture, air, and the material in vapor form, respectively; P is the total pressure $=p_h+p$; R the universal gas constant, and finally T denotes the absolute temperature given by $(\theta+\theta_0)[(P/P_0)^{R/MC_p}] \simeq \theta+\theta_0$, in which P/P_0 is approximately equal to unity for problems of current interest, which is fortunate since the last equation is strictly valid only when R/MC_p is constant.

Equations (1) and (2) were obtained by generalizing the anelastic approximation of Ogura and Phillips [8]. The essential features of the present (generalized anelastic) conservation equations are that variable density is allowed and yet sound waves are filtered *a priori* (thus time steps are not restricted by acoustic effects). The proper interpretations of neglecting $\partial\rho/\partial t$ in eq. (2) for mass conservation is that acoustic density variations in time are of very small amplitude and occur so quickly that it is a good approximation to assume density is always in equilibrium with the other thermodynamic variables. The time dependence of density is then determined implicitly by the time variation of temperature, pressure, and composition via the ideal gas law. It is not appropriate to interpret eq. (2) as implying $\partial\rho/\rho t = 0$ since ρ does indeed vary with time.

The above set of equations, together with appropriate initial and boundary conditions, are solved to obtain the fields of velocity, pressure, temperature, mass fraction of the dispersed material (in vapor and liquid phases), and den-

sity of the mixture as functions of time and space. For the dispersion simulations described herein, only natural gas (NG) vapor is being considered. Therefore the equation for liquid material (q_l) and the terms involving phase change and liquid material should be omitted.

2.2 Turbulence parameterization

The existing turbulence submodel in FEM3A is a K-theory local equilibrium model [4,7]. Since it was based on similarity theory of the atmospheric boundary layer over flat terrain and without obstruction, it is not appropriate for complex situations such as the source region or near the vapor fence/billboard. For instance, the presence of the fenced enclosure and billboard will generally result in turbulence enhancements; the spill mechanism (i.e., jetting of LNG onto the pond) will also create additional turbulence in the source area. Further complications are the presence of convective mixing inside the gas cloud caused by the much warmer water underneath. All these processes are indeed not treated by the existing submodel and are difficult to model accurately. For these reasons, an approach combining the existing variable K-model and constant diffusivities was used in the present study. Specifically, the existing K-model (with heavy-gas effects) was applied everywhere except within and near the vapor fence wherein the resulting turbulent mixing from all sources was parameterized with constant diffusivities. Justifications for taking the present simple approach include: (1) there was no validated, advanced turbulence submodel that could be readily adapted for the present spill scenarios, (2) developing a sophisticated turbulence submodel would require substantial effort beyond the scope of the present study, and (3) the lacking of sufficient experimental measurements on turbulence and heat transfer in the source area further hinders the development of a more sophisticated parameterization.

Currently the following *ad hoc* formula is used to estimate the value of diffusivities to be used (in all directions) within and near the fence enclosure:

$$K = CK_2 + V_i L\,, \tag{7}$$

in which the first term can be considered as representing the ambient turbulence modified by the presence of vapor/billboard and density stratification, the second term incorporates contributions related to the spill and source conditions. The respective symbols are: C is an empirical constant (currently taken to be 1.5), K_2 denotes vertical diffusivity at 2 m high in the ambient atmosphere, V_i the source injection velocity, and L the length scale (currently taken to be 8.7 m, the height of the vapor fence).

The above scheme of parameterization was adapted, based on a few 2-D simulations of the Falcon spill tests and a brief comparison of the simulated results with a limited amount of measured data in the spill area (no data outside of the fence was considered, however). Apparently, estimates based on such a formula are rather crude for the actual, complex turbulence mixing

process but they, nevertheless, appear reasonably well to represent the bulk of turbulent mixing occurring inside and near the vapor fence. As will be seen in Table 2, the second term (for contributions from the spill and source conditions) is a dominating factor for Falcon-1, is equally important as the first term for Falcon-2 and Falcon-3, and accounts for only one-third of the total diffusivity in the case of Falcon-4.

2.3 Source modeling and superheating effects

As pointed out by Waite et al. [9], the spread of a liquid on another liquid of greater density is difficult to describe mathematically. When the spreading liquid is a cryogen such as LNG, the simultaneous heat transfer and vaporization render the process even more intractable. Furthermore, experimental information on the concomitant heat transfer was rather incomplete. For instance, estimates of the heat flux from water to the liquefied gas pools have ranged over a factor of 4, from 25 to 100 kW/m^2. Although a fairly general pool spread and heat transfer model has been proposed and briefly tested against certain experimental results, adapting the model for the present applications is not a trivial task and the usefulness of such a model remains yet to be established.

For the above reasons, a simple approach has been taken in the present study. The current source submodel assumes that the spilled LNG evaporates as fast as it is spilled, uniformly in time and over the entire pond surface area. Additionally, depending on experimental evidence (such as the case of Falcon-1), extra heat flux may be supplied to superheat the vapor source. Currently, the superheating effects are modelled by adding a predetermined amount of heat flux (to the temperature equation) over the source area during the period of simulated spill.

The occurrence of superheating of the LNG source in Falcon-1 was strongly suggested by a number of field measurements. In Fig. 3, the measured temperature at 1 m above the water surface at the center of spill are displayed for the four Falcon tests (unfortunately, due to instrument failure, no data was available beyond 60 s for Falcon-3). Although the data for Falcon-3 are incomplete, it does seem true that a significantly lower temperature than all the other tests was realized. In contrast, the measured temperature of Falcon-1 is unusually high, despite this test having the highest spill rate. Specifically, its minimum temperature is 20°C above that of Falcon-2, almost 40°C higher than Falcon-3, and is comparable to that of Falcon-4. Another supporting evidence is presented in Fig. 4, which indicates an unusually large drop in water temperature near the center of spill ($\sim$8°C in this case versus $\sim$1.2°C for Falcon-4). A simple heat balance calculation reveals that, in order to vaporize all the LNG spilled, the water temperature in the spill pond has to drop merely 3.3°C. Although the entire body of water in the pond might not have cooled down uniformly by 8°C, the temperature was probably fairly uniform because there

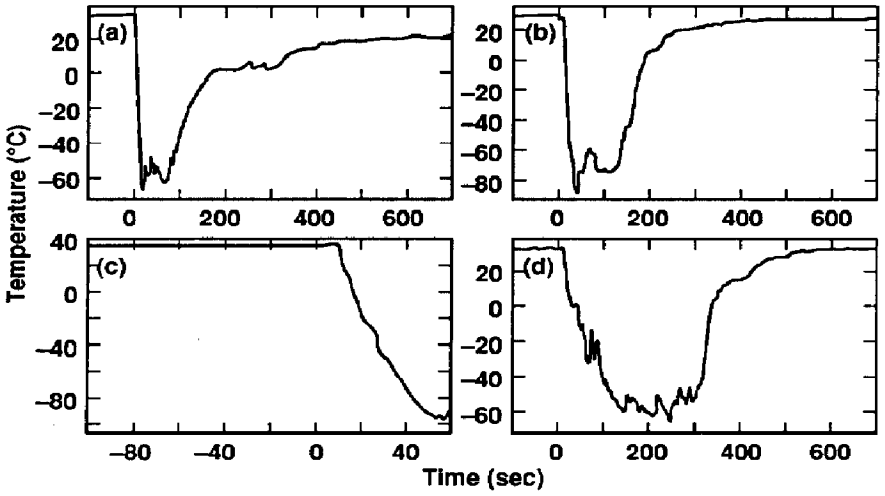

Fig. 3. Measured temperature inside the vapor fence at the center of spill and 1 m above the water surface for: (a) Falcon-1, (b) Falcon-2, (c) Falcon-3, and (d) Falcon-4.

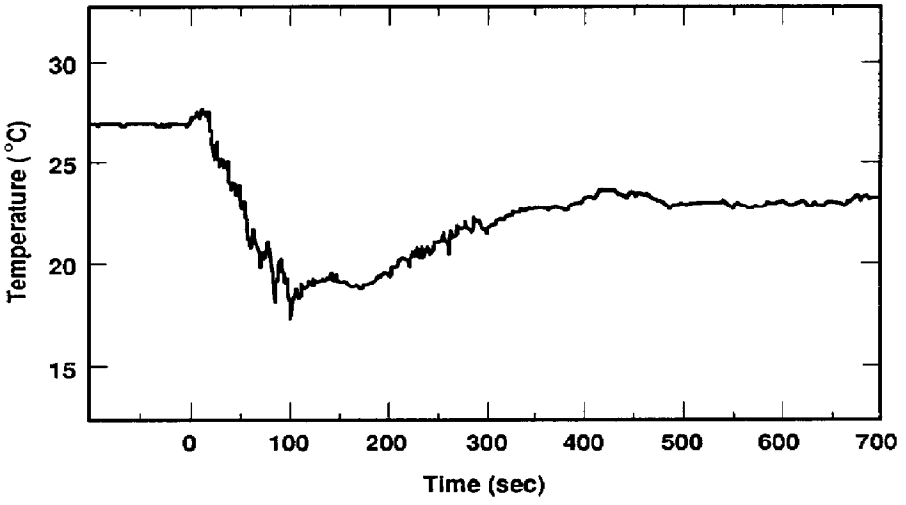

Fig. 4. Measured temperature at the center of spill and 5 cm beneath the water surface during the Falcon-1 spill experiment.

were circulation lines in the pond to keep the water fairly well mixed. Therefore, it is not inconceivable to expect the water to cool down 4 to 5°C on average, which is more than sufficient to provide the heat required to vaporize all the LNG spilled and the extra heat necessary to superheat the LNG source. One of our early 2-D calculations showed that the extra heat flux generated by 1°C drop in water temperature could make the vapor cloud 60°C warmer at 1 m above the water surface.

Indeed, more entrainments and turbulent mixing in Falcon-1 (due to its higher LNG exiting velocity—65 m/s vs 32.5 m/s for other tests) could also

help explain the unexpected results in Fig. 3. In this regard, a series of 2-D simulations with various levels of turbulence was conducted and the results indicated that very high values of diffusivities would be required in order to make the predicted concentration agree well with the measured data, but the corresponding temperature field generally remained much colder than observed. Although a further increase in diffusion could bring the predicted temperature to agree better with field data, however, the predicted concentrations would then fall far below the measured values. Therefore the reasoning of enhanced turbulence *alone* is not a satisfactory answer to the observed anomaly.

The possibility of superheated vapor was discussed in a pre-spill document by the Department of Transportation (DOT) [10], in which a vapor temperature increase between 10 to 35 °C was considered credible. Ruff et al. [11] also reported similar superheating phenomenon (with as much as 40 °C rise in vapor source temperature attributing to heat transfer from the bulk water underneath) in their laboratory experiments of confined spills of liquid nitrogen. It is conjectured that the high spill rate, low level of ambient turbulence, and relatively high water temperature are some of the factors that cause the Falcon-1 LNG source to be heated considerably above its boiling point, thus leading to the early overspillage of the vapor cloud in the field test.

2.4 Computational mesh

The computational domain for simulations with the presence of the fence enclosure is shown in Fig. 5. In order to conserve computing costs, the x–z plane was assumed to be the plane of symmetry, thus only one-half of the field was simulated in all cases. The domain is 370 m long (starting at 120 m upwind of the rear fence and ending at the 250 m row of gas sensors), 100 m wide (for one-half of the field in the crosswind direction), and 50 m high. The choice of such a computational domain and the associated mesh design were largely dictated by the desire to capture the most important flow/cloud structures and, at the same time, to keep the computing costs at a reasonable level (say, no more than 5 to 10 hours of computer time per simulation on a Cray-2 computer).

The domain was subdivided into 27,200 grid points ($85 \times 20 \times 16$ in the longitudinal, lateral, and vertical directions, respectively), distributed nonuniformly for higher cost-effectiveness. The minimum grid spacings were 0.4 m vertically and 1 m in the two horizontal directions. The maximum grid spacings were 10 m and 15 m, respectively. Even with such relatively fine grid spacings, the small-scale structures of the flow field such as the thin boundary layer near the fence (which was actually modelled as 1-m thick solid walls so as to avoid the stringent time step size and high computing cost otherwise required in the numerical simulations using a structured grid) and the ground are not expected to be well resolved. However, the large-scale structures of the flow and the cloud are believed to have been captured with reasonable accuracy.

In order to investigate the relative performance of the present vapor barrier,

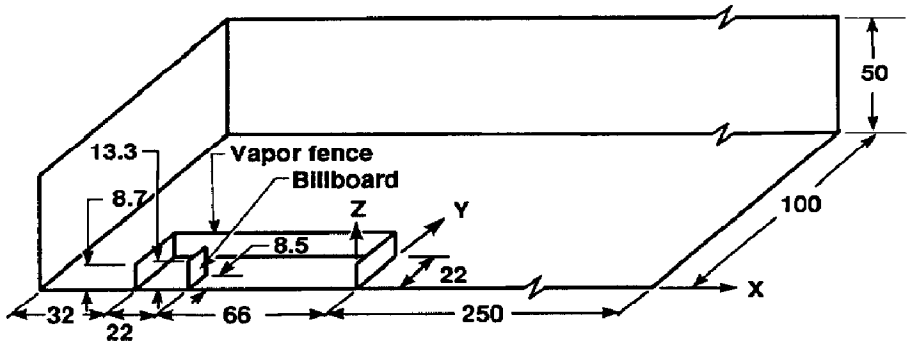

Fig. 5. Sketch of computational domain and dimensions (in meters) for one-half of the vapor fence and billboard. Vapor cloud is assumed to be symmetric about the x–z plane.

Falcon-4 was also simulated without the fence and the billboard. The computational domain was extended to 400 m downwind and a graded mesh consisting of 16,884 mesh points ($67 \times 18 \times 14$) was used.

3. Model-data comparisons

3.1 Simulated field tests

Five LNG vapor dispersion tests were conducted in the Falcon series of experiments [1]. During the last test, i.e., Falcon-5, large rapid phase transition (RPT) explosions occurred at approximately 60 s after the spill and a fireball started inside the vapor fence at 81 s. Because Falcon-5 has only limited data up to about 100 s for sensors outside of the fence, it was excluded from the present study. Listed in Table 1 are the spill and meteorological parameters of the selected tests.

The major characteristics of the tests are summarized below:

Falcon 1—This test had the highest spill volume and the highest spill rate (excluding Falcon-5) and was conducted under very stable atmospheric conditions. The vapor cloud in this test overflowed the vapor fence on all four sides in contrast to the pre-test wind tunnel simulation, which produced a vapor cloud essentially contained within the fence enclosure for all times. Although the sensor array was apparently too narrow to capture the entire cloud, very useful data are still available for model validation purposes. This test is markedly different from the rest of the tests, as it represents an LNG cloud dispersion resulting from high spill rate and calm wind conditions.

Falcon-2—This test had an intermediate spill rate and a relatively short spill duration 78 s), and was conducted under neutral ambient conditions. Unfortunately, due to internal software problems, only temperature measurements and concentrations data from the MSA gas sensors (mostly deployed at downwind locations and at 5 m high and above) are available.

Falcon-3—This test is more or less a repeat of Falcon-2, but with a spill dura-

TABLE 1

Spill and meteorological parameters

Test	Falcon-1	Falcon-2	Falcon-2	Falcon-4
Spill volume (m^3)	66.4	20.6	50.7	44.9
Spill rate (m^3/min)	28.7	15.9	18.9	8.7
Water temperature (°C) (pre/post spill)	28.4/22.4	23.6/20.6	no data	23.2/22.0
Temperature at 2 m (°C)	32.8	31.6	34.9	31.1
Avg. windspeed at 2 m (m/s)	1.7	4.7	4.1	5.2
Air pressure (mbar)	908.9	905.0	900.8	906.3
Pasquill stability class	G	D	D	D/E
Momentum diffusivity at 2 m (m^2/s)	0.0165	0.313	0.255	0.265
Richardson number at 2 m	0.1337	−0.0193	−0.0047	0.0252
Friction velocity (m/s)	0.0605	0.3565	0.3053	0.3694
Monin-Obukhov length (m)	4.963	−103.4	−422.2	69.38
Roughness length (m)	0.008	0.008	0.008	0.008

tion roughly twice as long (161 s). It produced a large quantity of good quality data; however, the test was plagued to some extent by significant RPTs, which started at approximately 60 s after the spill began.

Falcon-4—This test had the smallest spill rate, the longest spill duration (i.e. 310 s), and was conducted under neutral to slightly stable conditions. Due to its relatively long spill duration, this test could be considered, for most practical purposes, as having a continuous source with all the field variables reaching their respective steady state. Compared to the results of other tests, the data of this test appear to contain more high-frequency components (or more turbulent intermittency), because of its low spill rate and higher wind speed.

The spill and meteorological parameters used in the numerical simulations are given in Table 2. Since Falcon-2 is very similar to Falcon-3 and it does not have a complete set of concentration data, the focus herein will be on the remaining three tests, but with emphasis on Falcon-1 and Falcon-4. A more extensive model-data comparison can be found in Chan [6].

In the following, numerical results are compared with field data for the selected tests. The field data were taken at the rate of one samples but were averaged over five seconds for comparison with the numerical results. Such an averaging time is believed to be long enough for the turbulent time scales and yet is short enough for retaining the dynamical characteristics of the transient gas cloud. Both fields of concentration and temperature are considered and the comparison is conducted for locations both inside and outside of the vapor fence. Specifically, comparisons are made for time series of the field variables, the peak values of concentration along the cloud centerline, and contour plots of concentration on selected crosswind planes.

TABLE 2

Spill and meteorological parameters used in numerical simulations

Test	Falcon-1	Falcon-2	Falcon-3	Falcon-4
Area of source (m^2)	2400	2400	2400	2400
Injection velocity (m/s)	0.108	0.043	0.050	0.023
Duration of source (s)	100	78	161	310
Air pressure (N/m^2)	92,094	91,699	91,274	91,831
Reference temperature (K)	305.5	304.8	308.0	304.2
Friction velocity (m/s)	0.0605	0.3565	0.3053	0.3694
Monin-Obukhov length (m)	5.0	−103.4	−422.2	69.38
Wind profile (m/s)	_[a]	_[b]	_[c]	_[d]
Air temperature profile (°C)	$32.5+0.1z$	31.8	35.0	$31.2+0.05z$
Superheating (W/m^2)	9,600	0.0	0.0	0.0
Effective energy transfer velocity (m/s)	0.005	0.01	0.01	0.01
Water temperature (°C)	28.4	23.6	28.0	23.2
Diffusivity within fence and its vicinity (m^2/s)[e]	1.0	0.8	0.8	0.6

[a] $u(z)=0.8+0.4167z-0.01667z^2$ for $z<9$ m
$=3.2$ for $z\geq 9$ m.
[b] $u(z)=0.7466\,[\ln(1+z/0.008)+0.7694]$.
[c] $u(z)=0.6985\,[\ln(1+z/0.008)+0.3445]$.
[d] $u(z)=3.689+0.658z-0.0248z^2$ for $z<16$ m
$=7.877$ for $z\geq 16$ m.
[e] Based on eq. (7) and rounded to the nearest tenth.

3.2 Falcon-1

As indicated in Table 1, this test has the highest spill volume and spill rate, and was conducted under very stable atmospheric conditions. The mesh described in Section 2.4 was used, together with open lateral boundary conditions so as to allow the flow and the vapor cloud to leave the domain in a natural way. The existing K-model with heavy-gas effects was used everywhere except within and near the fence enclosure (defined by $x=-101$ to 30 m, $y=0$ to 26 m, and $z=0$ to 20 m in Fig. 5) wherein a constant K value of 1 m^2/s was used.

In this and all subsequent simulations, the vapor cloud was assumed to be symmetric about the center plane of the fence enclosure, thus only one-half of the vapor cloud was simulated. Such an assumption is apparently not very appropriate for Falcon-1 as evidenced by the significant deviation (about 20 degrees) of the wind trajectory from such a plane. However, tens of hours of Cray-2 time would have been required in order to simulate the entire cloud with similar grid resolution. Due to budgetary constraints and the uncertainty about the potentially gain in additional information, it was decided to postpone such an endeavor for future studies. Nevertheless, the present simulation is

still quite useful, both qualitatively and quantitatively, in improving the understanding of the vapor dispersion involving a vapor fence and under calm wind conditions.

In Fig. 6, the predicted gas concentration and velocity projection on the 1-m horizontal plane at 120 s (after spill began) are depicted. The gravity spreading of the cloud in the crosswind direction can be clearly seen Fig. 6(a). At this time, the vapor cloud already reached the lateral boundary. These results appear to correlate well with what was observed in the field experiment, i.e, a vapor cloud overfilling the fence enclosure and spreading out quickly after the spill started. Illustrated in Fig. 6(b) are the much altered velocity field (which was nearly unidirectional over a much larger area under ambient conditions) due to the presence of the dense cloud. Owing to stable density stratification, the flow field within the fence is largely quiescent. Because of its high spill rate and calm wind conditions, Falcon-1 has apparently produced the most profound perturbation to the ambient atmosphere among all the Falcon tests.

In Fig. 7, the predicted concentration for a location near the fence side is compared with measurements taken by a Jet Propulsion Laboratory sensor, which unfortunately is the only operational gas sensor inside the vapor fence

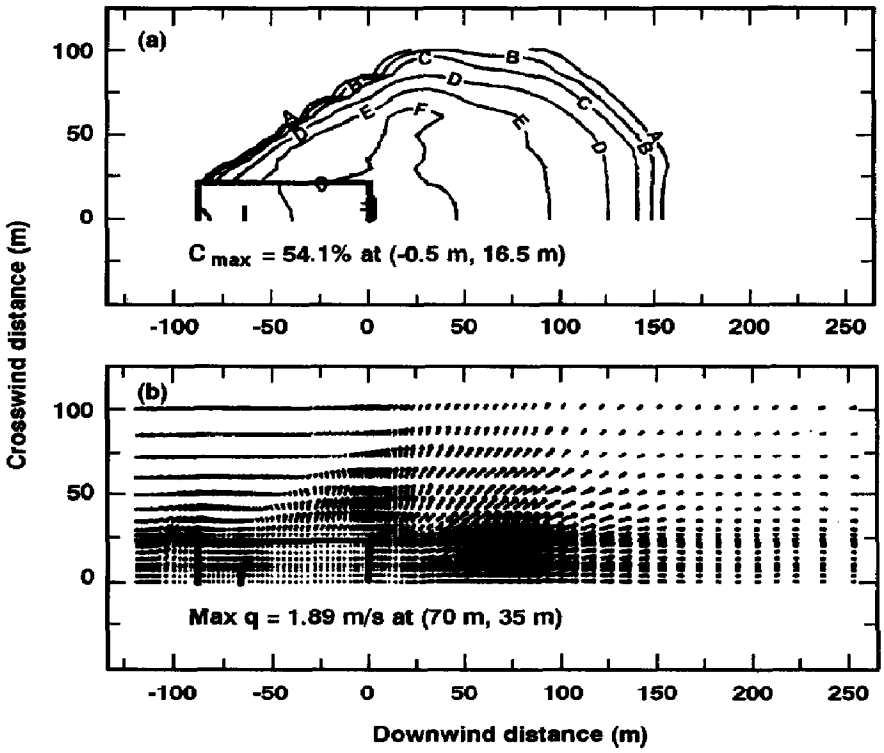

Fig. 6. Falcon-1 predicted concentration contours and velocity projection on the horizontal plane 1 m above the ground surface after 120 s. The contour levels are (in vol.%): A=0.5, B=1, C=2, D=5, E=10, F=15, G=25, H=35, and I=50.

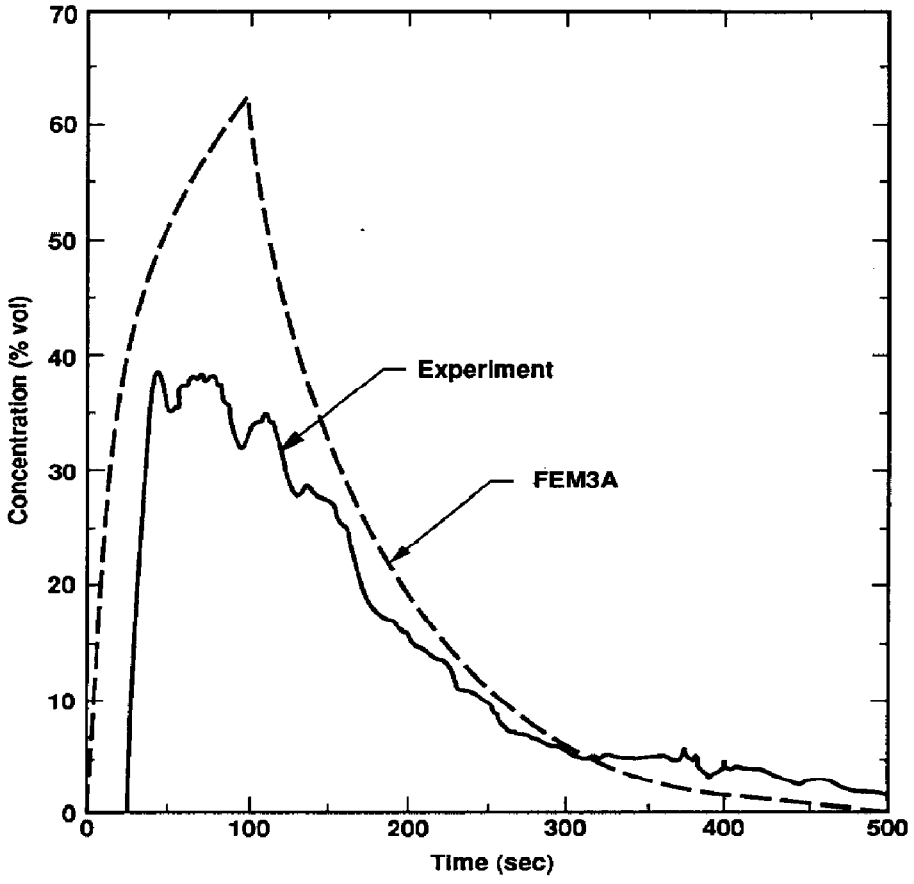

Fig. 7. Falcon-1 predicted versus measured concentration for two locations within and near the fence side. The predicted values are for location at $(x,y,z) = (-60$ m, 20 m, 1 m) and the measurements are for location at $(x,y,z) = (-62$ m, 20 m, 1 m).

for this test. Despite the fact that FEM3A overpredicts peak value of the concentration (61% vs. 39%), the shapes of the two curves, nevertheless, agree reasonably well. The discrepancy in the cloud arrival times is attributable to the simplicity of the constant area source submodel. The discrepancy in the peak values is partly due to the slight difference in the two locations being compared (data was taken at 2 m further away from the center of spill) and partly due to the simple source submodel. More sophisticated modeling of the source conditions, including turbulence and heat transfer, is considered to be important in obtaining a closer agreement.

In Fig. 8, the predicted concentration for two different heights at 50 m are compared with data measured near the cloud centerline. Considering the complexities of the vapor dispersion phenomena, the overall agreement between model predictions and field data is fairly good. In particular, the predicted results for the 1 m high location appear to agree quite well with field measurements, with respect to the overall shape of the curves, the peak values, and cloud arrival/departure times, etc. For the location at 5 m high, the actual vapor cloud was much less coherent than predicted by the numerical model.

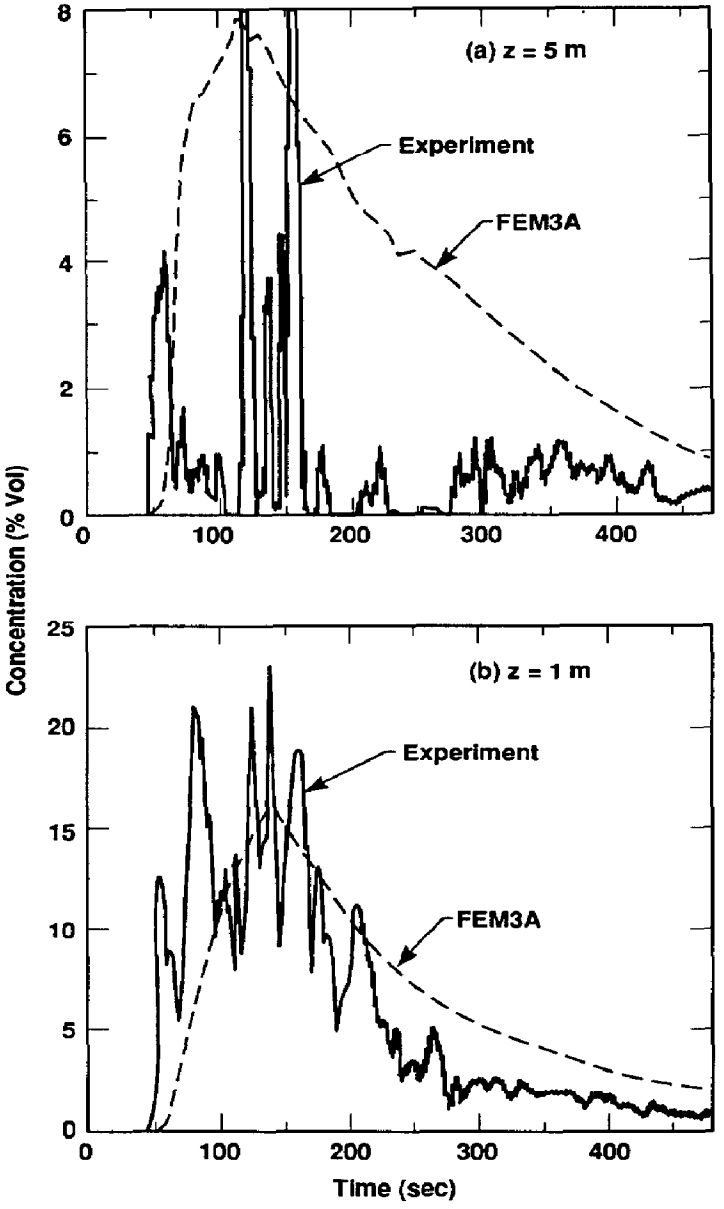

Fig. 8. Falcon-1 predicted versus measured concentration for two different heights at 50 m behind the rear fence. The predicted values are from locations on the vertical plane of symmetry and the measurements are from gas sensor G04 (which is near the cloud centerline).

The large discrepancies at this location are believed mainly due to the presence of the less stable cloud/air interface in that vicinity (see Fig. 9 for the actual height), coupled with a rather coarse ($\sim$2 m) grid spacing nearby. Also, the discrepancies might have been aggravated by the model's assumption of symmetry (as opposed to the actual unsymmetric cloud) and the considerable distance between the gas sensors considered and the actual cloud centerline.

The predicted and measured concentration contours for the crosswind plane at 150 m downwind are shown in Fig. 9 at 300 s, assuming the cloud centerline

to be at −45 m (based on the information of wind trajectory). As seen in this figure, the numerical model predicts somewhat higher concentration on the ground and an "average" cloud height of ~6 m (for the 0.5% concentration contour), which is comparable to the experimental value of approximately 5 m. Unfortunately, it is not possible to compare the cloud width, because the cloud at this time already went beyond the edges of the sensor array and the computational domain. The gap (between −36 m and −54 m) in the actual cloud is near the cloud centerline and is probably a manifestation of cloud bifurcation due to significant gravity spreading and misalignment of the centerlines of the cloud and the fence enclosure. In the present numerical simulation, only a weak bifurcation was hinted for the higher concentration contours (2% and 5%) but it became more apparent at 480 s (not shown here).

Finally, the maximum values of concentration along the "cloud centerline" are compared in Fig. 10 (due to significant cloud bifurcation of Falcon-1, it is more appropriate to compare the predicted centerline values against the measured values at similar locations, rather than the measured peak values over the entire crosswind plane). Overall, the model is underpredicting the concentration as much as 35% relatively. Considering the symmetry assumption and the simple approach used to model the source conditions, including superheating and turbulence inside the fence, such discrepancies are perhaps within reasonable expectations.

3.3 Falcon-3

The Falcon-3 test is basically a repeat of Falcon-2 with a slightly higher spill rate and approximately twice as long in spill duration. Unfortunately, the oc-

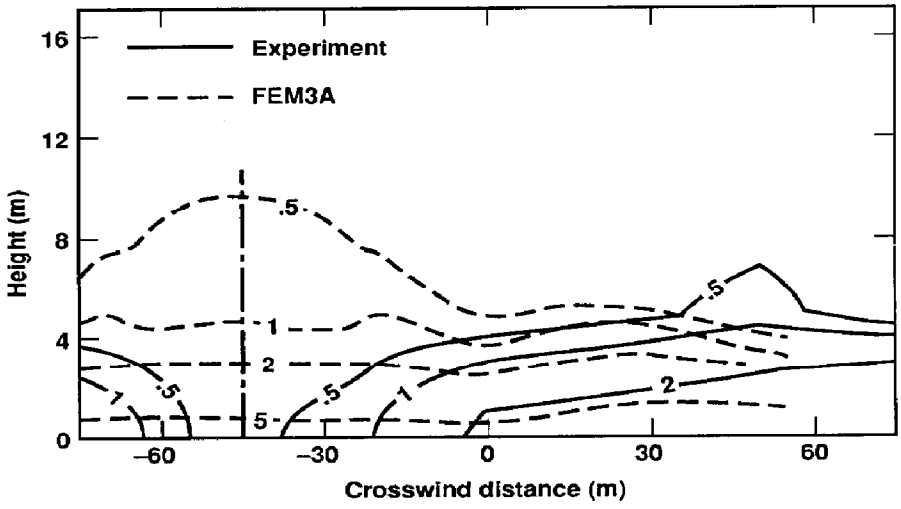

Fig. 9. Falcon-1 predicted versus measured concentration contours (in vol.%) on the crosswind plane 150 m behind the rear fence at a time of 300 s.

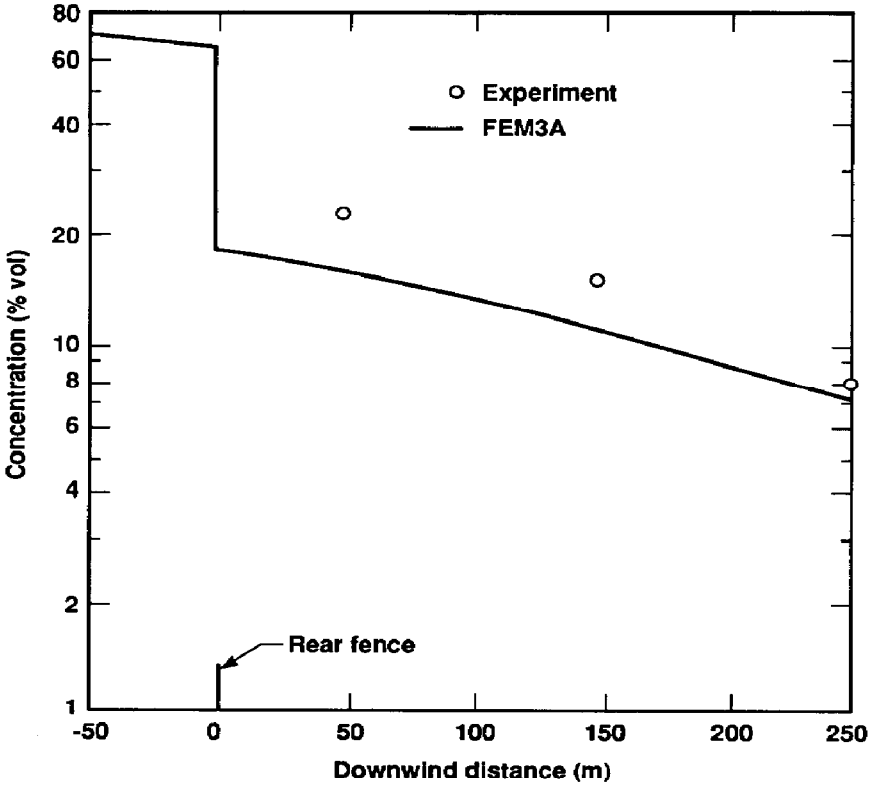

Fig. 10. Falcon-1 predicted versus measured maximum concentration along the cloud centerline and at 1 m high.

currence of many RPTs during the early stage of spill caused some of the instruments inside the vapor fence to malfunction, thus greatly reducing the amount of field measurements available for comparison. Nevertheless, a fair amount of data are still largely valid for comparison purposes. The main results for this test are compared in Figs. 11 through 13.

In Fig. 11, the predicted time-series of concentration for two different heights at 150 m are compared with field data. The numerical results are very consistent and generally correlate quite well with field data, regarding cloud arrival/departure times, magnitude of the concentrations, and the shapes of the curves (indeed, the high-frequency components due to small eddies not adequately modeled must be neglected).

The predicted and measured concentration contours for the crosswind plane at 150 m behind the rear fence are compared in Fig. 12 at a time of 240 s. As is seen, the predicted cloud is fairly low (slightly below 10 m), and is very wide (with a half-width of nearly 100 m). The corresponding experimental results indicate a similarly low but perhaps somewhat wider cloud. If the cloud centerline is considered to be at −30 m, as presently assumed based on the wind trajectory, the measured cloud half-width at this time would be more than

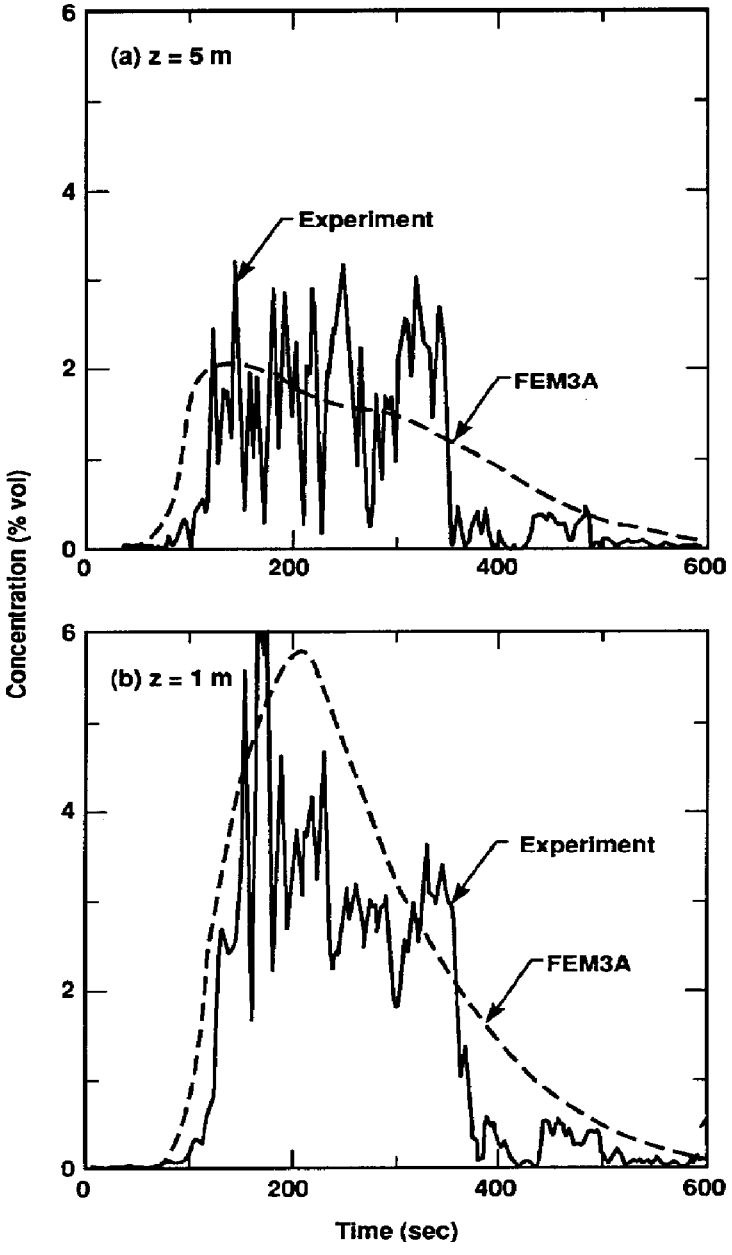

Fig. 11. Falcon-3 predicted versus measured concentration for two different heights at 150 m behind the rear fence. The predicted values are from locations on the vertical plane of symmetry and the measurements are from gas sensor G12 (which is near the cloud centerline). In (b), experiment has a spike of 7.6% at a time of 160 s.

100 m. Despite the model prediction of a somewhat narrower cloud (probably) and slightly higher concentration near the ground surface, the overall agreement between model predictions and field measurements appears to be very good, especially for the heights of the concentration contours.

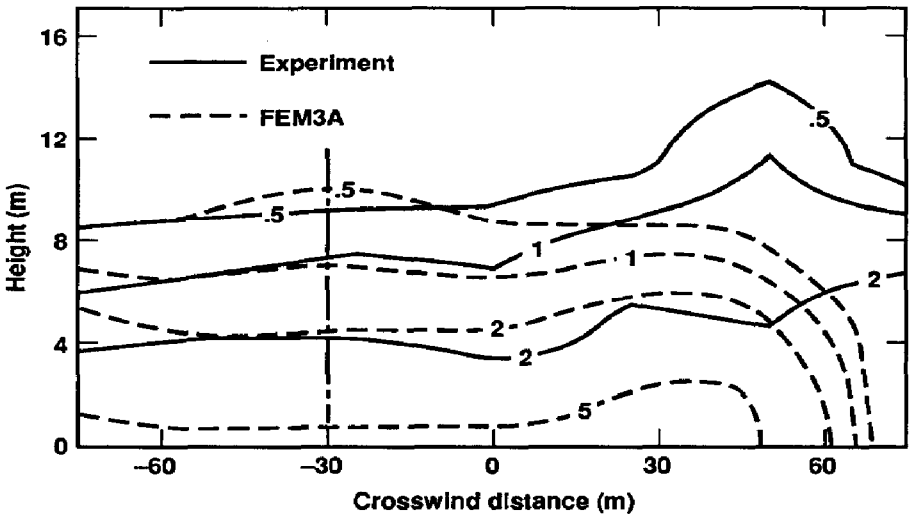

Fig. 12. Falcon-3 predicted versus measured concentration contours (in vol.%) on the crosswind plane 150 m behind the rear fence at a time of 240 s.

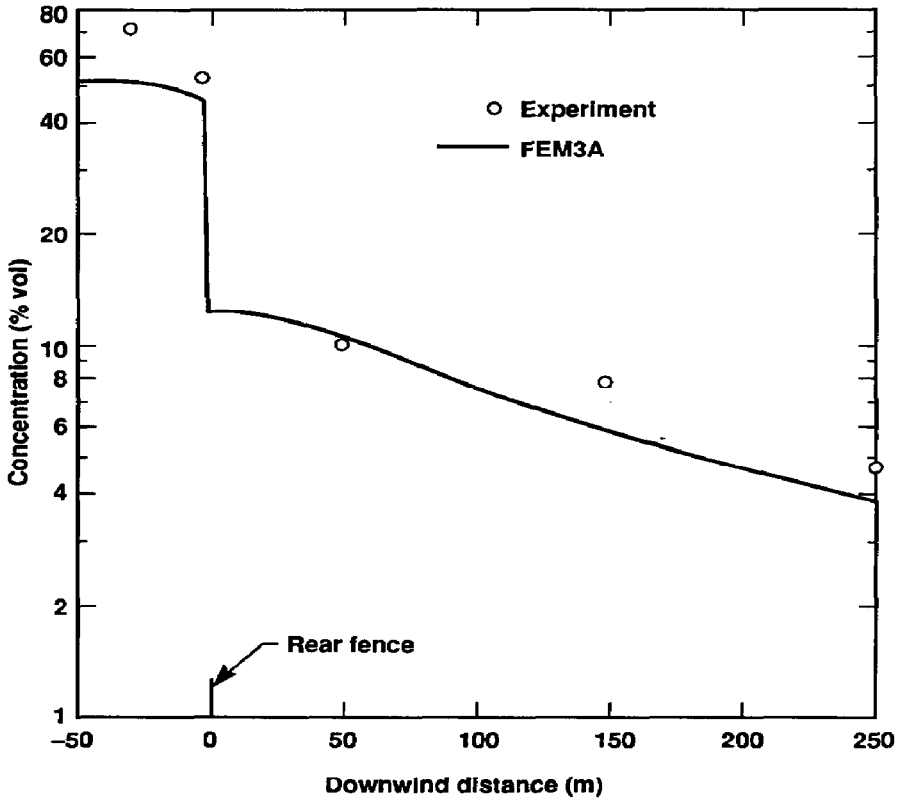

Fig. 13. Falcon-3 predicted versus measured peak concentration in the downwind direction and at 1 m high.

In Fig. 13, the predicted peak concentrations along the cloud centerline and at 1 m high are compared with field measurements. Again, the agreement is very good with regard to the concentration values and their variation in the downwind direction. The unusually high value of concentration measured near the center of spill at $x = -32$ m is very likely due to a less homogeneous cloud created by RPTs and/or due to sensor problems prior to its complete failure after a time of 175 s.

3.4 Falcon-4

In this test, 45 m^3 of LNG was released over a period of 310 s under neutral ambient conditions with an average wind speed of 5.2 m/s. The relatively low spill rate, long spill duration, and nearly steady atmospheric conditions made this test behave like a continuous spill. In order to evaluate the relative performance of the fence enclosure, two simulations were performed for this test: one with the fence/billboard and one without.

In Fig. 14, the steady state results of concentration at a time of 300 s from the two simulations are compared. Although the two clouds are both fairly wide and low, their shapes are quite different. The vapor fence has produced a cloud with its height varying from 20 m to slightly below 10 m and its half-width expanding to almost 65 m at 250 m downwind. Without the fence enclosure, the cloud started out with a wedge-shaped leading edge, which is a result of the density front opposed by the shear stresses near the ground, and evolved to nearly 12 m high only. This cloud was dispersed downwind much quicker and its values of concentration near the ground are generally much higher. Additionally, due to the lack of lateral confinement, this cloud tends to spread out immediately in the source region and results in a wider and lower cloud thereby. Also revealed in this figure is the potential effectiveness of a vapor fence. For instance, the downwind distance to the 2.5% concentration on the ground was reduced from approximately 380 m to 235 m and a substantial reduction in the hazardous area enclosed by the 2.5% concentration contour was also achieved.

In Fig. 15, the predicted and measured time series of concentration near the center of spill are compared. The numerical results (with vapor fence) are very consistent and correlate quite well with the measured data, regarding the magnitude and cloud persistence time. During the duration of LNG spill, results from the two numerical simulations are fairly close, implying the domination of the spill conditions over the fence effects at such a location. However, after the spill has been terminated (after 310 s), the curves are drastically different regarding cloud persistence and concentration level. For instance, the concentration is above 2.5% for approximately 530 s in the case with vapor fence, as opposed to 330 s without the vapor fence. These results suggest that, in spite of its advantages, e.g., reducing the level of concentration, delaying cloud arrival time, and curtailing the downwind distance of hazardous area, an LNG vapor fence could significantly prolong the cloud persistence time within the

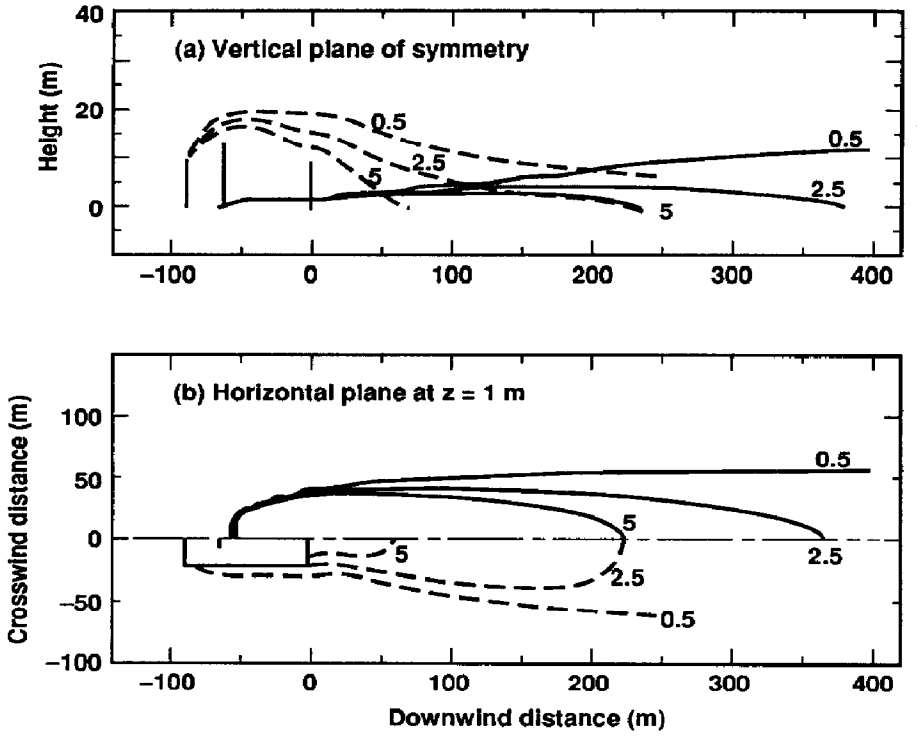

Fig. 14. Falcon-4 predicted concentration contours (in vol.%) at time = 300 s from two simulations: with vapor fence (– – –), and without vapor fence (—).

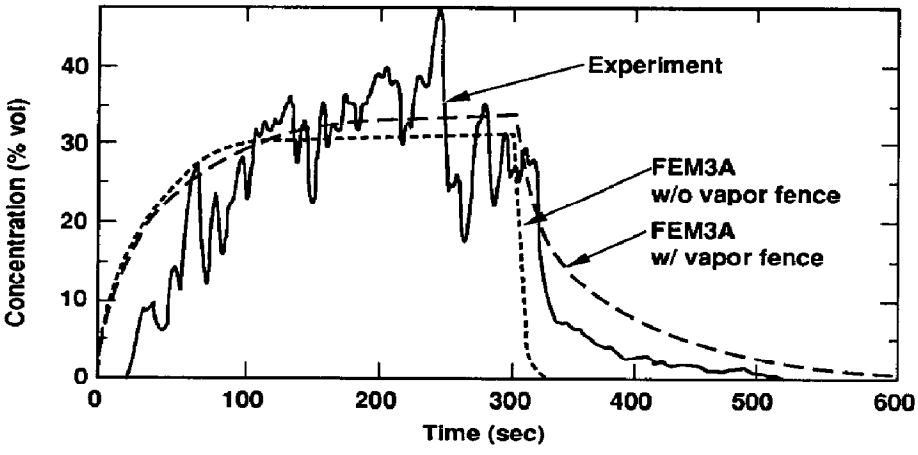

Fig. 15. Falcon-4 predicted versus measured concentration at the center of spill and 1 m above the water surface.

fence, thus increasing the potential for ignition and combustion in such an area.

In Fig. 16, the predicted time-series of concentration are compared with field data for two different heights at 150 m. Again, the numerical results are very consistent and generally correlate very well with field data, regarding cloud arrival/departure times, peak concentration values, and the shapes of the curves.

The predicted and measured concentration contours on the crosswind plane at 150 m behind the rear fence are compared in Fig. 17 for a time equal to 300 s, with the cloud centerline assumed to be at −35 m. The hump in the experimental results is probably due to the presence of a puff of cloud passing through the 11 m high gas sensor. As is seen, the predicted cloud height is roughly the same as observed. However, the predicted cloud width is considerably narrower than that of the actual cloud and the predicted concentration near the ground is slightly higher. Besides experimental uncertainties, most of the discrepancies are probably a combined result of the inadequacy of the turbulence submodel and the assumption of a symmetric vapor cloud. Meroney and Shin [12] also reported a considerably narrower cloud (a width of ~120 m based on 1% concentration) in wind tunnel simulations and observed that, even with small wind orientation variations (8° and 10°), the vapor cloud profiles differ significantly.

In Fig. 18, the predicted peak concentrations (with vapor fence) along the cloud centerline and at 1 m high are compared with field measurements. The agreement is very good with regard to the concentration values and their variations in the downwind direction, in spite of the larger discrepancies on the cloud width noted above. This fact suggests that a comparison of centerline concentrations, though useful and of practical interest, is generally insufficient in assessing the performance of a model. Other measures such as the cloud profiles and time series of the field variables should also be duly considered. Also superimposed in the figure are the results of a simulation without the vapor fence and the billboard. Without such structures, the concentration would have been nearly twice as high at 250 m and four times higher at 50 m. The downwind distance to the 2.5% concentration would have been 365 m, instead of 230 m.

3.5 Comparison via the ratio method

In this subsection, the overall performance of the numerical model is assessed via applying the ratio method to the predicted and measured field variables, as recommended by Ermak and Merry [13] to all four tests. Included in such direct comparison are: the maximum drop in temperature, cloud arrival and persistence times for certain concentration levels of practical importance, the peak values of concentration, and the maximum down-wind distances to concentrations of 2.5% and 5% (the lower flammability limit of LNG). The relevant values are obtained from the time series of temperature and concentration presented in Chan [6] for the locations listed in Tables 3 and 4.

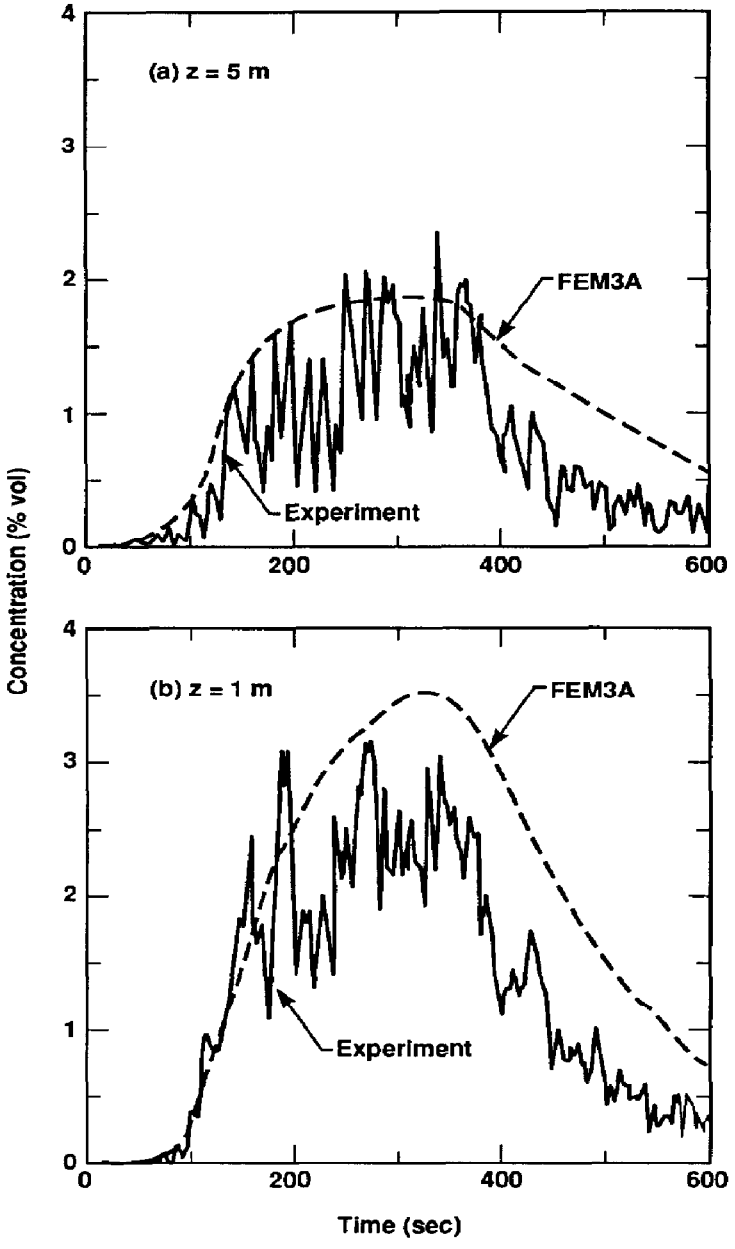

Fig. 16. Falcon-4 predicted versus measured concentration for two different heights at 150 m behind the rear fence. The predicted values are from locations on the vertical plane of symmetry and the measurements are from gas sensor G02 (which is near the cloud centerline).

In Fig. 19, the cloud arrival and persistence times for concentrations of 1% and 2.5% at sample locations behind the vapor fence are depicted. With only a few exceptions, the predicted values are within a factor of 2 (mostly within 1.5) of the measured values. The exceptions include those locations at 5 m high in the Falcon-1 test (with data point for location [150 m, 0 m, 5 m] being out

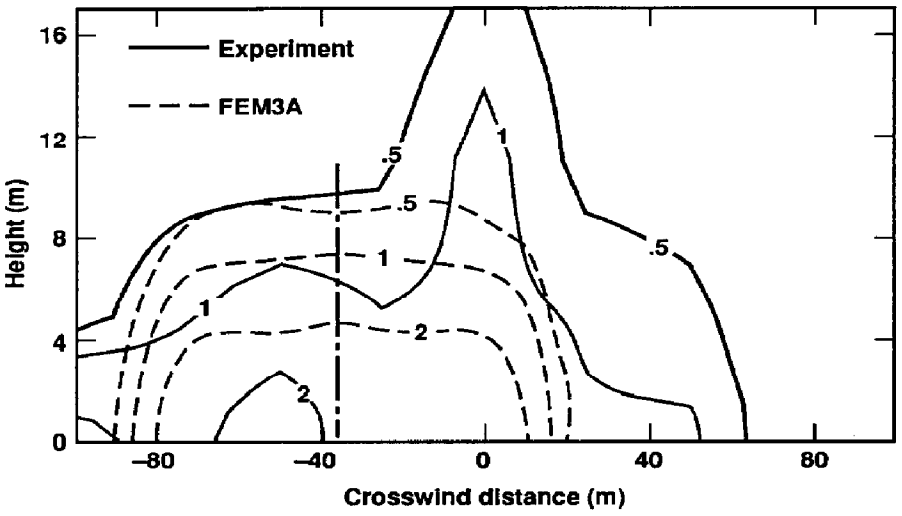

Fig. 17. Falcon-4 predicted versus measured concentration contours (in vol.%) on the crosswind plane 150 m behind the rear fence at a time of 300 s.

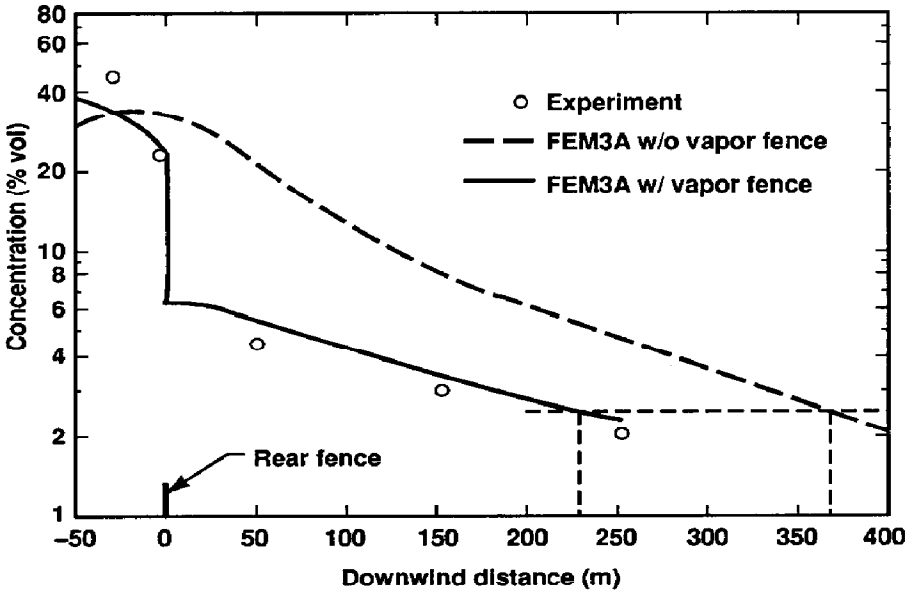

Fig. 18. Falcon-4 predicted versus measured peak concentration in the downwind direction and at 1 m high.

of the figure), where a cloud/air interface with large gradients exists and is thus more difficult to predict well, and the location of (250 m, 0 m, 1 m) in Falcon-2, wherein significant cloud meandering appears to have occurred.

The predicted versus observed maximum decreases in temperature and the peak values of concentration at all sampled locations, both inside and outside of the vapor fence, are plotted in Fig. 20. As is seen in Fig. 20(a), all the data

TABLE 3

Locations for model-data comparison of temperature

(x,y,z) in meters	Falcon-1	Falcon-2	Falcon-3	Falcon-4
(−32, 0, 1)	×	×		×
(−2, 0, 1)	×	×	×	×
(50, 0, 1)	×	×	×	×
(50, 0, 5)	×	×	×	×
(150, 0, 1)	×	×	×	
(150, 0, 5)		×	×	

TABLE 4

Locations for model-data comparison of concentration

(x,y,z) in meters	Falcon-1	Falcon-2	Falcon-3	Falcon-4
(−62, 0, 1)		×	×	
(−62, 20, 1)	×	×		
(−32, 0, 1)		×	×	×
(−2, 0, 1)			×	×
(50, 0, 1)	×		×	×
(50, 0, 5)	×		×	×
(150, 0, 1)	×		×	×
(150, 0, 5)	×		×	×
(250, 0, 1)	×	×	×	×
(250, 0, 5)	×	×	×	×

points are bounded by a ratio between $\frac{1}{2}$ and 2, with the majority falling within the range of $\frac{2}{3}$ and 1 $\frac{1}{2}$. With one exception of the data point (which in outside of the figure) for location (150 m, 0 m, 5 m) of Falcon-1 for reasons alluded to earlier, similar model performance is observed in Fig. 20(b) for the peak values of concentration.

Finally, the predicted versus measured maximum downwind distances for concentration of 2.5% and 5% are tabulated in Table 5. Except for Falcon-2, which did not have concentration data at 1 m high for the 50 m and 150 m rows, results from all the remaining three tests were compared. Of the six values of ratio, five of them are within a factor of 1.5, and the remaining one is slightly larger than 2 for the distance of the 5% concentration of Falcon-4.

4. Concluding remarks

In this study, the FEM3A model has been modified slightly and applied to simulate four large-scale LNG vapor barrier field experiments. A fairly de-

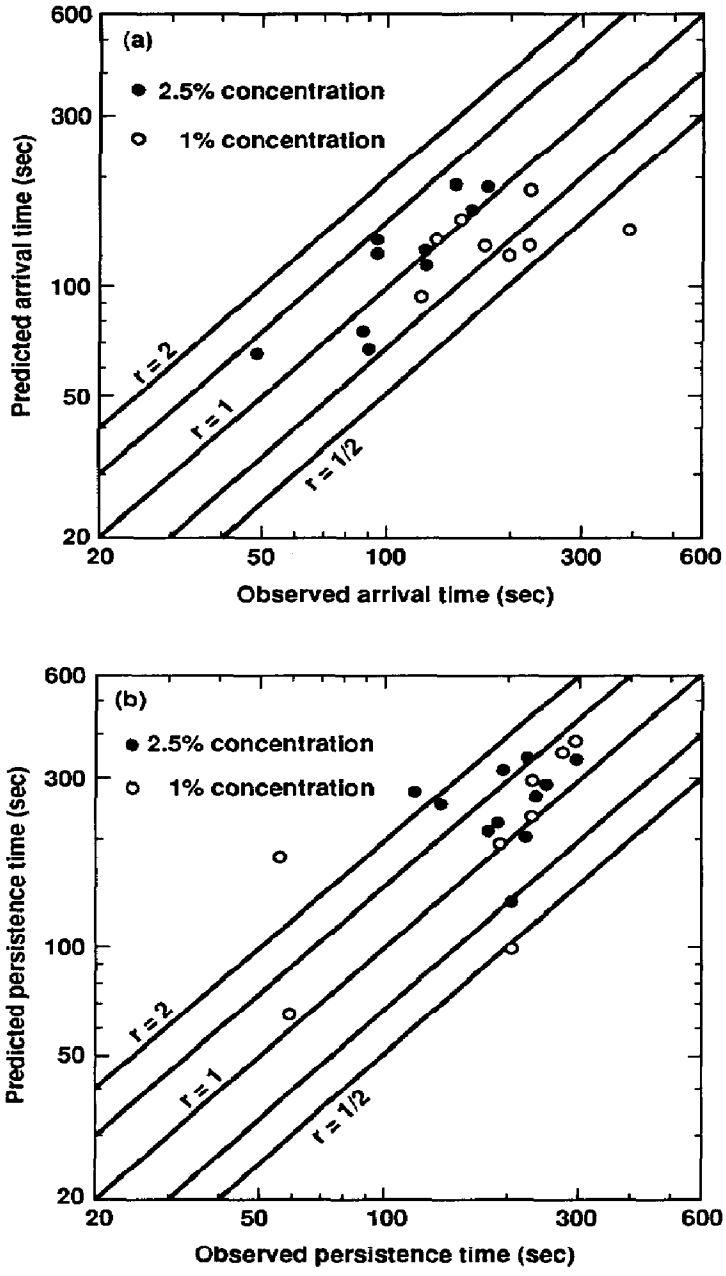

Fig. 19. Predicted versus observed cloud arrival and persistence times for concentration higher than 1% and 2.5% at sample locations behind the vapor fence.

tailed model-data comparison was made to evaluate its performance. The following are conclusions and recommendations based on the numerical results and a comparison with available field data.

(1) The FEM3A model, with minor modifications, is able to reproduce the major results of the vapor barrier field tests with reasonable accuracy. Specif-

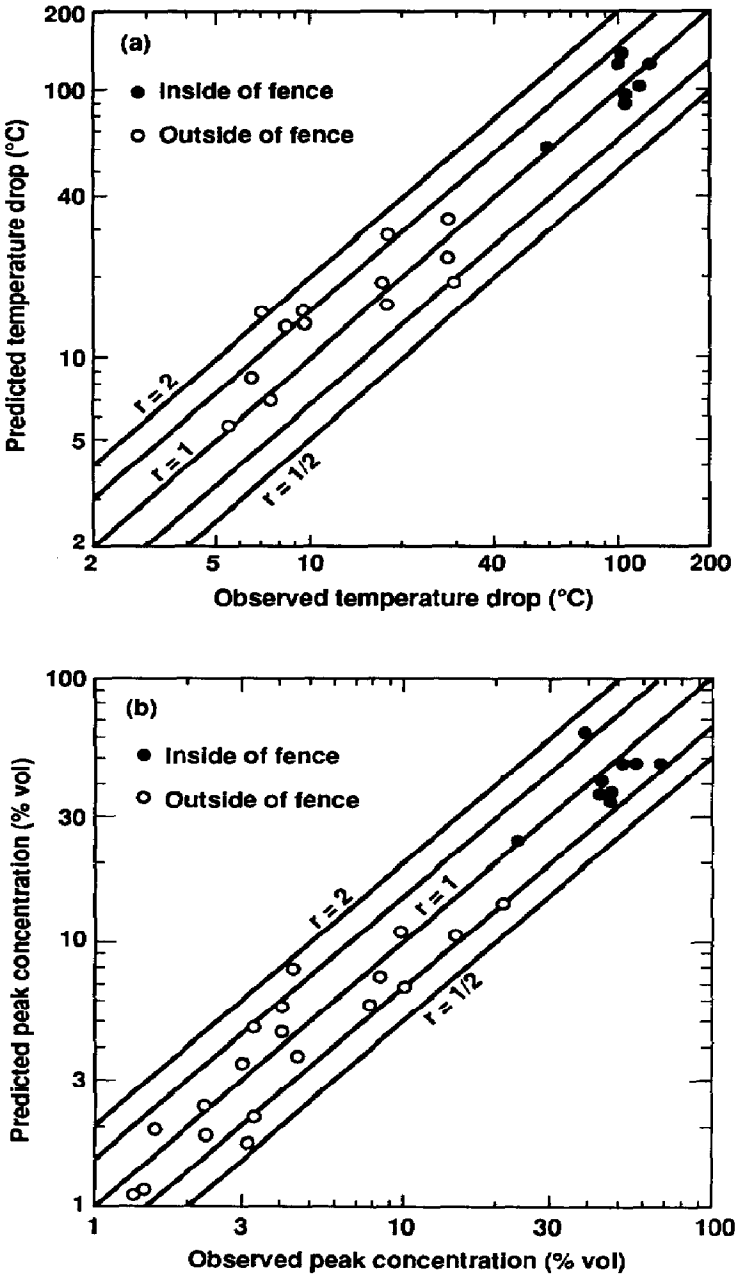

Fig. 20. Predicted versus observed maximum decreases in temperature and peak values of concentration at sample locations inside and outside of the vapor fence.

ically, a comparison between the predicted and measured variables, including the maximum change in temperature, the peak values of concentration, representative cloud arrival and persistence times, and the downwind distances to concentration of 2.5% and 5%, was made and the majority of the results agree well within a factor of two.

TABLE 5

Predicted versus measured maximum down-wind distances (in meters, measured from the rear fence) for concentration of 2.5% and 5%

Test	Model	2.5% Data	Ratio	Model	5% Data	Ratio
Falcon-1	498	440	1.13	340	330	1.03
Falcon-2	200	N/A	-	70	N/A	-
Falcon-3	330	353	0.93	183	230	0.80
Falcon-4	230	203	1.13	65	28	2.32
Falcon-4 (no fence)	365	N/A	-	230	N/A	-

N/A means 'not available'.

(2) The predicted results of Falcon-1 are consistent with field observations, i.e., a vapor cloud overfilling the fenced enclosure, in contrast with a vapor cloud essentially contained within the fence at all times as observed in a pre-spill wind tunnel simulation. The surprising results of the Falcon-1 test are believed partly due to the greatly enhanced turbulence mixing (mainly induced by the extremely high LNG exiting velocity) and partly due to superheating of the LNG source by the water underneath. Although certain field data appear to substantiate the above claims, insufficient measurements of concentration and temperature in the source area do not allow a more definite conclusion. If technically possible, laboratory experiments are highly recommended for testing the superheating hypothesis.

(3) Based on the numerical results from simulations with and without the fenced enclosure for Falcon-4, an LNG vapor fence was observed to have the following advantages: significantly reduced concentration in the near field, delayed cloud arrival times at downwind locations, and a much shortened downwind distance of hazardous area. However, a vapor fence could also prolong the persistence time of the vapor cloud in the source area, thus increasing the potential for ignition and combustion within the vapor fence and the area nearby.

(4) Since the actual centerline of the Falcon-1 vapor cloud was about 20° off the center plane of the instrumentation array, the present assumption of the vapor cloud being symmetric about the center plane of the sensor array is not strictly valid. A full domain simulation with the correct mean wind direction is necessary for a more appropriate model-data comparison. Such a simulation would require substantial computer resources but is, nevertheless, computationally feasible and recommended to be performed in future studies.

(5) Due to the complexity of the source conditions, which generally involve LNG pool spread, heat transfer and evaporation, and perturbations to turbulent mixing in the ambient atmosphere, etc., such processes have been parameterized with relatively simple submodels. Although such an approach ap-

pears to have performed reasonably well, the predicted cloud widths were generally narrower than observed. More sophisticated modeling of the source conditions and turbulent mixing may be necessary in order to simulate the cloud dispersion accurately at all locations. This is particularly true for the case of Falcon-1 wherein the dispersion process appears to be largely dominated by the spill conditions and the obstruction of the fence/billboard.

(6) All the simulations presented herein were performed without the presence of water vapor. Although humidity did not appear to be a crucial factor for unconfined LNG spills such as the Burros and Coyotes [3], its effects were relatively significant in the marine environment [14] and may prove to be important for the present spills involving vapor barriers, especially under the conditions of the Falcon-1 experiment. A humidity submodel should probably be implemented in FEM3A for future investigation of such effects.

Acknowledgements

This work was performed under the auspices of the U.S. Department of Energy by the Lawrence Livermore National Laboratory under Contract W-7405-Eng-48. The funding for this study was provided by the Gas Research Institute (GRI) under contract No. 5088-252-1704. Ted Williams was the GRI project manager. Raylene Cooper skillfully typed the manuscript.

References

1 Gas Research Institute. Falcon Series Data Report: 1987 LNG Vapor Barrier Verification Field Trials, GRI Report No. 89/0138, Chicago, IL, June 1990.
2 R.E. Britter, Atmospheric dispersion of dense gases, Annu. Rev. Fluid Mech., 21 (1989) 317–344.
3 S.T. Chan and D.L. Ermak, Recent results in simulating LNG vapor dispersion over variable terrain, In: G. Ooms and H. Tennekes (Eds.), Proc. of the IUTAM Symp. on Atmospheric Dispersion of Heavy Gases and Small Particles, Springer-Verlag, Berlin, 1984, pp. 105–114.
4 S.T. Chan, D.L. Ermak and L.K. Morris, FEM3 model simulations of selected Thorney Island phase I trials, J. Hazardous Mater., 16 (1987) 267–292.
5 S.J. Wiersma and T.A. Williams, Vapor fences for LNG dispersion control, AGA Operating Section Proc., American Gas Association, Arlington, VA, 1990, pp.557–561.
6 S.T. Chan, FEM3A Simulations of Selected LNG Vapor Barrier Verification Field Tests, Lawrence Livermore National Laboratory, UCRL-CR-105184 (also GRI-90/0189), Livermore, CA, October 1990.
7 S.T. Chan, FEM3A—A Finite Element Model for the Simulation of Gas Transport and Dispersion: User's Manual, Lawrence Livermore National Laboratory, UCRL-21043, Livermore, CA, April 1988.
8 Y. Ogura and N. Phillips, Scale analysis of deep shallow convection in the atmosphere, J. Atmos. Sci., 19 (1962) 173–179.
9 P.J. Waite, R.J. Whitehouse, E.B. Winn and W.A. Wakeham, The spread and vaporization of cryogenic liquids on water, J. Hazardous Mater., 8 (1983) 165–184.

10 U.S. DOT, Large LNG Spills Verification Field Trials, U.S. Department of Transportation, Washington, DC, 1985.
11 M. Ruff, F. Zumsteg and T.K. Fanneløp, Water content and energy balance for gas cloud emanating from a cryogenic spill, J. Hazardous Mater., 19 (1988) 51–68.
12 R.N. Meroney and S.H. Shin, LNG Vapor Barrier and Obstacle Evaluation: Wind tunnel Post-field Test Program, GRI LNG Project Advisor Group Meeting, Fayetteville, AR, November 1990.
13 D.L. Ermak and M.H. Merry, A Methodology for Evaluating Heavy-Gas Dispersion Models, UCRL-21025, Lawrence Livermore National Laboratory, Livermore, CA, September 1988.
14 G.W. Colenbrander and J.S. Puttock, Maplin Sands experiments 1980: Interpretation and modeling of liquefied gas spills onto the sea, In: G. Ooms and H. Tennekes (Eds.), Proc. of the IUTAM Symp. on Atmospheric Dispersion of Heavy Gases and Small Particles, Springer-Verlag, Berlin, 1984, pp. 277–295.